



Soft Matter

Self-assembly of amphiphilic polymers of varying architectures near attractive surfaces

Journal:	<i>Soft Matter</i>
Manuscript ID	SM-ART-10-2019-002104.R1
Article Type:	Paper
Date Submitted by the Author:	18-Nov-2019
Complete List of Authors:	Wessels, Michiel; University of Delaware, Chemical and Biomolecular Engineering Jayaraman, Arthi; University of Delaware, Chemical and Biomolecular Engineering & Materials Science and Engineering

SCHOLARONE™
Manuscripts

(submitted to Soft Matter)

Self-assembly of amphiphilic polymers of varying architectures near attractive surfaces

Michiel G. Wessels¹ and Arthi Jayaraman^{1,2,}*

*1. 150 Academy Street, Colburn Laboratory, Department of Chemical and Biomolecular Engineering,
University of Delaware, Newark, DE 19716, USA*

2. Department of Materials Science and Engineering, University of Delaware, Newark, DE 19716, USA

† Electronic Supplementary Information (ESI) available: Criteria for defining adsorbed chains and clusters; assembly results away from surfaces/in the bulk solution; solvophobic block persistence lengths; additional assembled structure results with differing number of coarse-grained beads per chain and different surface patterns.

See DOI: 10.1039/x0xx00000x

***Corresponding author E-mail:** arthij@udel.edu

Abstract

We use coarse-grained molecular dynamics simulations to investigate the assembly of A-B amphiphilic polymers near/on surfaces as a function of polymer architecture and surface attraction to the solvophobic B-block in the polymer. We study four polymer architectures: linear, bottlebrush with a backbone that is longer than each of the side chains, bottlebrush where the solvophobic backbone is similar in length to each of the side chains, and ‘star-like’ architectures where the backbone is significantly shorter than the side chain lengths. For each architecture and surface-B attraction, we quantify the assembled aggregate structure (*i.e.*, aggregation number, domain shapes and sizes) and the chain conformations (*i.e.*, components of the chain radius of gyration) on and away from the surface. For all the architectures and surface-B attraction strengths, the assembled structure away from the surface is similar to the assembly observed in bulk systems without surfaces. Near/on the surface, the assembled B-blocks form domains whose shapes and sizes are dependent on the surface-B attraction strength and the ability of the B-block in the polymer architecture to change conformations and pack on the surface. Domain sizes formed from linear and ‘star-like’ polymer architectures show the most sensitivity to surface-B-block attraction strength, transitioning from hemispherical to disordered domains with increasing attraction strength. In contrast bottlebrushes with long backbones and short side chains transition from hemispherical to striped to continuous domains with increasing surface-B attraction strength. Bottlebrushes with similar solvophobic backbone and side chain lengths form hemispherical domains that do not change significantly with the surface-B-block attraction strength. These computational results can guide experimentalists in their choices of surface chemistry and polymer architecture to achieve desired assembled domain shapes and sizes on the surface.

1. Introduction

Assembly of linear and branched block copolymers on surfaces have been shown to be useful in microelectronics, lithography, sensors, optics and photonics, as described in many review articles.¹⁻⁶ The type of application dictates the desired shapes and sizes of the self-assembled domains. For example, continuous domains with sharp interfaces are preferred for applications involving transport (*e.g.*, microelectronics, microfluidics), and patterns of spherical nanoscale domains with regular spacing are preferred for optics and photonics. Previous experimental and computational studies have described ways to control self-assembly of block copolymers on the surface by tuning the polymer-surface and the polymer-polymer interactions through the choice of the polymer, solvent and surface chemistry as well as the polymer architecture.¹⁻⁶ Even though a large portion of the previous work is on linear polymers, in the past few decades, non-linear or branched polymer architectures, such as bottlebrushes, have begun to receive more attention (see review articles¹⁻⁶). The bottlebrush architecture is comprised of a linear backbone with densely grafted side chains. The steric hinderance between the densely grafted side chains along the backbone result in an extended polymer whose shape (*e.g.*, worm-like) and stiffness depend on the ratio of their backbone and side chain lengths.⁷⁻⁹ Various experimental, computational, and theoretical studies^{2, 10-18} have investigated the conformations of bottlebrushes and comb copolymers architectures. The studies focused on polymer adsorption on surfaces find that the polymer architecture affects the conformations more significantly on surfaces than in the bulk as the reduced volume available for the side chains increases their steric repulsion along the backbone. Additionally, these studies find that the competition between the backbone and side chain interactions with the surface can lead to non-trivial adsorption behavior.

The impact of the conformational features of the bottlebrush polymer on their self-assembly has been studied in solution,¹⁹⁻³⁸ in bulk,³⁹⁻⁴³ as well as at surfaces.^{42, 44-50} Bottlebrush copolymers close to surfaces have been shown to have faster assembly kinetics and form ordered domains with larger sizes without the use of additives as compared to linear copolymers.⁴⁵⁻⁴⁸ Deposition of bottlebrush copolymers also leads to a variety of stimuli-responsive surfaces that come from different arrangements of

functional groups within the bottlebrush chemistry, that preferentially assemble at or away from the surface depending on the solvent conditions.^{46, 49, 50} The above useful studies have elucidated the behavior of bottlebrushes in solution and on surfaces, but to the best of our knowledge there are no studies that systematically vary the polymer branching (*e.g.*, from linear to bottlebrush or comb polymer to star polymer) to show how increasing/decreasing crowding of the side chains along the polymer backbone impacts the self-assembly near surfaces, specifically the domain shapes, domain sizes, and chain conformations on surfaces.

In this paper, we use coarse-grained (CG) molecular dynamics (MD) simulations to investigate the self-assembly of different amphiphilic block copolymer architectures on surfaces with varying strengths of attraction to the solvophobic B-block. We study architectures ranging from linear to bottlebrushes to ‘star-like’; ‘star-like’ are essentially bottlebrushes with short backbone and few long side chains. In the bottlebrush and ‘star-like’ cases we vary the side chain grafting density (*i.e.*, number of side chains per backbone bead) from 1 to 4. This study on surfaces is an extension of our previous study⁵¹ on self-assembly of some of these architectures in solution in the absence of the surface. In that study, we found that both the solvophobicity required for assembly of the copolymers and the assembled micelles’ aggregation number varied non-monotonically with the polymer architecture going from linear to bottlebrush to star-like. This non-monotonic trend was linked to how the topological arrangement of the solvophobic B-segments within the copolymer architecture hindered/aided solvophobic contacts in solution. In this paper, we find that the polymer architecture and grafting density dictates how easy/difficult it is for the B-segments within the polymer chains to reorganize on the surface to make energetically favorable surface-B contacts. This impacts the shape of the assembled domain on the surface and the sensitivity of the domain shapes and sizes to different surface-B attraction strengths. Bottlebrushes with a long backbone and short side chains are stiffer near surfaces than in bulk, due to the increased steric hindrance from the side chains of adsorbed polymers. These stiffened bottlebrush polymers pack more regularly to form continuous or striped domains at higher surface-B interaction strengths. Bottlebrushes with similar solvophobic backbone and side chain

lengths form hemispherical domain structures, that due to the stiffness described above, do not change with varying surface-B attraction strength. In contrast, linear and ‘star-like’ polymer architectures maintain their flexibility and adopt different energetically favorable configurations depending on the surface-B attraction strength, forming different domain shapes that are sensitive to the surface-B attraction strength. Increasing the grafting density in the non-linear architectures increases the topological constraint on the chains deterring them from adopting different chain conformations; in most cases hemispherical domain structures are formed for all values of surface-B attraction strengths in this study.

The rest of this paper is organized as follows. In section 2, we present the model, the simulation and analyses methods, and discuss the design parameters varied in this study. In section 3, we discuss our results of the self-assembly of various polymer architectures on different solvophobic surfaces. In section 4, we summarize our results and discuss the implications of our findings.

2. Methods

2.1. Model

To represent generic A-B amphiphilic copolymers with varying architectures we use a coarse-grained (CG) bead-spring model^{52, 53} similar to our previous work.^{51, 54} All CG polymer beads, backbone and side chain, have a diameter of 1σ , a mass of $1m$, and are bonded with a harmonic spring with a force constant of $50\epsilon/d^2$ and an equilibrium distance of 1σ ; all values are expressed in reduced Lennard-Jones (LJ) units.⁵⁵ The polymer backbone and side chains are modeled as flexible chains with no imposed angle potential. This generic CG model with backbone and side chain beads of the same size and a flexible polymer backbone is chosen to fairly compare assembly behavior of the different polymer architectures, some comprised mostly of backbone beads (*e.g.*, linear polymer with no side chains) and others of mostly side chain beads (*e.g.*, ‘star-like’ polymer).

We model the solvent implicitly and capture its effect on the solvophobic (B) components with a LJ potential,⁵⁵ where the strength of the B-B LJ potential, ϵ_{BB} , captures different solvent qualities. Increasing

values of ϵ_{BB} indicate that the solvent quality is becoming poorer for the solvophobic component and drives the self-assembly of the amphiphilic copolymers. The LJ potential has a cutoff of 2.5σ and is shifted to have a value of 0 at and above the cutoff distance. All interactions with the solvophilic (A) beads are modeled to be in a good solvent with the Weeks-Chandler-Andersen (WCA) potential⁵⁶ with a cutoff of $2^{1/6}\sigma$ and is shifted to have a value of 0 at and above the cutoff distance. These features of the model are the same as we used in our recent publication,⁵¹ where we investigated bulk solution polymer assembly without surfaces. In that paper we also discussed briefly how this type of CG model could be mapped to specific polymer chemistries and solvent mixtures.

In this work, we represent the surfaces at the top and bottom simulation boundaries in the z direction with square-packed two-dimensional arrays of CG beads of the same size as the polymer beads (**Figure 1**). All other boundaries of the simulation box (*i.e.*, in x and y directions) maintain periodic boundary conditions. We model the bottom surface of the simulation box as attractive towards the solvophobic B-block of the polymer and model the top surface of the simulation box as a neutral non-attractive surface. To model the attraction of the bottom surface towards the B-block of the amphiphilic polymer, we incorporate a cut and shifted LJ potential with attraction strength, ϵ_{WB} , shifted to have a value of 0 at and above the cutoff distance of 2.5σ . To model the interactions of top neutral surface to the A- and B-beads, and the bottom surface to the A-beads, we use the repulsive-only WCA potential shifted to have a value of 0 at and above the cutoff distance of $2^{1/6}\sigma$. We choose to model the surface through explicit surface beads instead of an effective surface-polymer potential (*e.g.*, Ref.⁵⁷) to facilitate future studies on chemically or physically patterned surfaces. The explicit surface beads also represent realistic experimental systems where the surface attraction towards the B-block would be engineered via functionalization of the surface with B-polymer/oligomers.

2.2. Simulation details

Similar to our recent publications,^{51, 58-61} in this paper, we use MD simulations in the NVT ensemble with the LAMMPS package⁶² to capture the self-assembly of the amphiphilic copolymers in dilute

solutions. We maintain the temperature using the Nosé-Hoover thermostat.⁶³ We simulate a system of 600 polymers placed in a simulation box with an occupied volume fraction (η) of 0.025 excluding the surface beads. The x and y dimensions of the simulation box are equal and restricted to integer multiples of the surface bead size to prevent unphysical overlap at the periodic boundaries. The z dimension (simulation box height) is adjusted to achieve the η of 0.025. The box size and system size (*i.e.*, number of chains in the box) are selected to allow for enough chains in the solution to form micelles without a complete depletion of chains from the solution to the surface. Additionally, the box height or the distance between the top and bottom surfaces in the z direction is large enough to ensure we observe bulk-like assembled morphologies in the region away from the attractive surface (as described in the results section).

We create our initial configuration by randomly placing the 600 polymer chains. To prevent overlap of these polymers with the top and bottom surface beads, we place the CG polymers within the center of the simulation box in the z direction, where we define the center as a distance that is equal to 20% of the box height away from both surfaces). To relax away from this initial configuration, we simulate this system for 3,000,000 timesteps at $T^*=4.0$ with $\epsilon_{BB}=0.3$ and $\epsilon_{WB}=0.3$, where the LJ interaction strengths are below what is required for polymers to assemble. After this mixing stage, we set the temperature of the simulation to $T^*=1.0$ and allow the system to equilibrate for another 3,000,000 timesteps. Using this configuration, we begin our gradual stage-wise increase of the solvophobicity (ϵ_{BB}) to drive the self-assembly of the amphiphilic copolymers and achieve equilibrated configurations at each value of ϵ_{BB} . This gradual increase in ϵ_{BB} is similar to experiments where a second solvent that is poor for the solvophobic block is added to an existing polymer solution. We spend 3,000,000 timesteps at each value of ϵ_{BB} and increase ϵ_{BB} with increments of 0.005 until assembly does not change with increasing ϵ_{BB} . The number of timesteps spent at each value of ϵ_{BB} and the increments in ϵ_{BB} are tested with replicate simulations where we increased the number of timesteps at each ϵ_{BB} (longer equilibration times) to ensure that results are reproducible and at equilibrium at each value of ϵ_{BB} .^{51, 56, 59, 62}

To mimic different surface chemistries, we vary the attraction strength of the surface to the

solvophobic B-bead, ϵ_{WB} . We either fix this interaction strength ϵ_{WB} throughout the simulation even as ϵ_{BB} changes (protocol 1) or increase both ϵ_{BB} and ϵ_{WB} simultaneously and keep them equal throughout the simulation (protocol 2), as shown in **Figure 2**. The former represents surface chemistries that are not significantly sensitive to changing solvent quality, and thus, surface interactions with the solvophobic B-block do not change as the solvent condition becomes poor for the B-block in the polymer. The latter is a case where the surface is coated with the same chemistry as the solvophobic B-block of the polymer.

2.3. Analyses

We analyze the assembled structures, both in the solution away from the surface (*i.e.*, bulk) and on the surfaces, visually and by calculating the aggregation number and size of the assembled structure. We also determine the chain conformations of the polymer chains adsorbed to the surface.

To identify the chains as either adsorbed to the surface or being in solution, we first calculate concentration profiles of the centers of mass of the solvophobic B-block as a function of perpendicular distance from the attractive surface. In the concentration profiles, at high values of ϵ_{WB} (*i.e.*, after all clusters have assembled both near and far from the surface), we identify two separate regions – one comprised of the center of mass of the solvophobic B-blocks near/on the surface and another comprised of the center of mass of the B-blocks that are away from the surface, as shown in **Figure S1**. The distance from the surface that separates the two regions is chosen as the cutoff distance and the chains with center of mass of the B-block below this cutoff distance are considered to be adsorbed on the surface.

We identify assembled clusters near/on the surface and away from the surface based on the distance criteria defined above. We define chains to be part of a cluster if they have a minimum number of neighbors within a critical distance between the center of mass of the solvophobic blocks. We show how we determine the critical distance and the minimum number of neighbors in **Figure S2**. The critical distance is determined from the solvophobic B-block center of mass radial distribution function after the clusters have formed (**Figure S2a**). The large values of the radial distribution function at low r denote the micelle core. The critical distance is chosen as the smallest value of r where the radial distribution function approaches the

bulk value of 1. From the probability distribution of the number of neighbors that each solvophobic B-block has within the critical distance, we identify the minimum number of neighbors as the value for which the probability reaches zero, as shown in **Figure S2b**. After determining which chains are neighbors, we use a ‘friends of friends’ algorithm,⁶⁴ to calculate the number of clusters. We also calculate the average number of chains in each cluster i , $N_{agg,i}$, (*i.e.*, the aggregation number) at each value of ϵ_{BB} for the n number of clusters formed at that ϵ_{BB} . We follow this procedure separately for clusters formed on the surface and in the bulk solution.

To determine the radius of gyration of the hemispherical domains formed on the surface, we calculate for each domain the center of mass of the solvophobic B beads that are within 1σ from the surface. From this center of mass, we determine the radius of gyration of the hemispherical domain i

$$R_{g,i}^2 = \frac{1}{N_{agg,i}N_{tot}} \sum_{j=1}^{N_{agg,i}} \sum_{k=1}^{N_{tot}} (\mathbf{r}_{jk} - \mathbf{r}_{cm,i})^2 \quad (1)$$

where \mathbf{r}_{jk} is the position vector of bead k in chain j and $\mathbf{r}_{cm,i}$ is the position vector of the center of mass on the surface of the hemispherical cluster defined above. We then calculate the average squared radius of gyration shown in Equation 1 over all the hemispherical domains for that system. Additionally, we visualize snapshots of the domains formed on the surface during the simulation using VMD.⁶⁵ We show all of the beads as well as only the solvophobic B-beads to view the solvophobic domains formed on the surface without obstruction.

To understand the conformations that the polymer chains adopt parallel and perpendicular to the surface, we calculate the parallel ($R_{g,B,\parallel}^2$) component and the perpendicular ($R_{g,B,\perp}^2$) component of the radius of gyration of the solvophobic B-block. We report the average values from all chains adsorbed to the surface.

2.4. Design parameters explored

We consider a range of polymer architectures keeping the total number of beads fixed at $N_{\text{tot}} = 96$. For all architectures studied in this paper, the total number of beads in a chain, N_{tot} , can be calculated from the number of backbone beads per chain (N_{bb}), the number of side chain beads per side chain (N_{sc}) and the grafting density of side chains on the backbone (*i.e.*, the number of side chains per backbone bead, z) as

$$N_{\text{tot}} = N_{\text{bb}}(1 + zN_{\text{sc}}). \quad (2)$$

As we explore linear, bottlebrush, and ‘star-like’ architectures (shown in **Figure 3**), we keep the N_{tot} constant by decreasing N_{bb} and simultaneously increasing N_{sc} at a side chain grafting density of $z = 1$, where each backbone bead has one side chain. For each of the architectures studied for $z = 1$ we also present results at an increased side chain grafting density of $z = 4$, where each backbone bead has four side chains; this leads to different values of N_{tot} from left to right in the bottom row in **Figure 3**.

In protocol 1 (**Figure 2**), we investigate $\varepsilon_{\text{WB}} = 0.35, 0.40, 0.45, 0.50, 0.55, 0.65, 0.70$, and 0.80 for polymer architectures with $z = 1$. As polymer architectures with $z = 4$ have many more beads than their counterparts with $z = 1$, they are able to make a higher number of B-bead contacts with the surface at lower values of ε_{WB} . Thus, for polymer architectures with $z = 4$, we investigate $\varepsilon_{\text{WB}} = 0.30, 0.35, 0.40, 0.45, 0.50$, and 0.60 .

Lastly, we investigate two different bead packing arrangements on the surface: two-dimensional square-packed and hexagonal-packed lattices. For the square-packed surfaces, we follow both simulation protocols while for hexagonal-packed surfaces, we only investigate select systems to show that the pattern does not affect the structure, but only the values of ε_{WB} at which different domains form.

3. Results & Discussion

Before focusing on our results near/on the attractive surface, we present evidence that the assembled structure of the polymers away from the surface is not impacted by the presence of a surface or the surface attraction strength to the B-beads. For all cases covered in this study, we observed spherical micelles in the bulk (away from the surface) and the aggregation numbers of the micelles for all architectures with $z = 1$ and $z = 4$ are not affected by the absence or presence of the surface and value of ε_{WB} (**Figure S3 and S4**). Similarly, the micelle core size and the total micelle size (see **Figure S3 and S4 parts b and c**) also remain unaltered in the bulk by the presence of the surface and its attraction to the B-beads. For polymers with $z = 1$, we see the same non-monotonic pattern in the aggregation number, micelle core size, and total micelle size with changing polymer architecture going from linear to bottlebrush to ‘star-like’ at a fixed number of beads per chain, as discussed in our recent publication on solutions without surfaces.⁵¹ In that publication, we showed that the non-monotonic trend in aggregation number arises from how the topological arrangement within a polymer affects the ability of the polymer to pack and make energetically favorable contacts with other chains within a micelle. For polymers with $z = 4$, we do not see the same non-monotonic pattern in the aggregation number with changing polymer architecture as seen for $z = 1$. Instead, we see that the ‘star-like’ architecture behaves more like a bottlebrush. The non-monotonic trend in $z = 1$ polymers arises because the ‘star-like’ polymer architecture with $N_{bb} = 4$ and four side chains has far less steric repulsion among the side chains and packs more chains efficiently into a micelle than is possible with the $z = 4$ ‘star-like’ polymer architecture with $N_{bb} = 4$ and sixteen side chains.

Now we focus our results and discussion on the complex interplay of the polymer architecture and the surface chemistry (ε_{WB}) on the assembled structures near/on surfaces. For $z = 1$ polymers, when we use protocol 1, as the value of the ε_{WB} is increased from 0.35 to 0.65 (each a different simulation), the number of assembled domains on the surface, and the size and aggregation number within each of the assembled domains increase (see visually in **Figure 4** and quantitatively in **Figure 5**). At the lowest value of ε_{WB} , ε_{WB}

$= 0.35$, assembled domains form on the surface only for the linear architecture (noted as architecture 1 in **Figures 4 and 5**). At each fixed value of ϵ_{WB} , the size of the assembled domains decreases as the polymer architecture changes going from linear to bottlebrush (architectures 1 and 2 to 4) and then increases going from bottlebrush to ‘star-like’ polymer architectures (architectures 4 to 5). This is seen clearly for $\epsilon_{WB} = 0.55$ and 0.65 . These changes in assembled domain size with varying polymer architecture are similar to the trend observed for micelle sizes in bulk in the absence of the surface, as discussed in the previous paragraph. In **Figure 5**, we quantify this non-monotonic pattern in the adsorbed assembled domain sizes as a function of the polymer architecture and find that this pattern is exaggerated as the value of ϵ_{WB} increases; the linear polymer architecture shows the largest increase in aggregation number and domain size with increasing values of ϵ_{WB} , while bottlebrushes with short side chains ($N_{bb}=32$ $N_{sc}=2$ and $N_{bb}=24$ $N_{sc}=3$) and the ‘star-like’ ($N_{bb}=4$ $N_{sc}=23$) polymer architectures form domains with a subdued increase in aggregation numbers and domain sizes. Interestingly, in the results presented in **Figures 4 and 5**, the polymer architecture that shows the least sensitivity to surface chemistry (*i.e.*, value of ϵ_{WB}) is the bottlebrush with similar solvophobic backbone and side chain length ($N_{bb}=12$ $N_{sc}=7$). For this polymer architecture (**Figure 5a and 5b**) both the aggregation number and size of the hemispherical domains on the surface remain fairly similar with varying values of ϵ_{WB} . Based on this one could conclude that if one wishes to obtain consistent hemispherical patterns for a broad range of different surface-B interactions, one should choose an architecture where the backbone of the solvophobic block and the side chains are similar in length.

At values of $\epsilon_{WB} > 0.65$, depending on the polymer architecture we see either an order-order transition (hemispheres to stripes on surfaces) or a transition from ordered hemispherical domains to inter-connected domains. For $\epsilon_{WB} = 0.65$ and 0.70 in **Figure 4**, the bottlebrushes with short side chains ($N_{bb}=32$ $N_{sc}=2$) and the ‘star-like’ ($N_{bb}=4$ $N_{sc}=23$) polymer architectures form connected hemispherical domains or stripes similar to the sphere to cylindrical transition in micelles formed in solution.⁶⁶ At $\epsilon_{WB} = 0.80$, these ordered hemispheres/stripes transition to inter-connected domains for all bottlebrushes (architectures 2, 3, and 4) and to disordered domains for linear and ‘star-like’ polymers (architectures 1 and 5, respectively).

Interestingly, visual comparison between the bottom two rows in **Figure 4** shows that this behavior is also found at $\varepsilon_{\text{WB}} = 0.80$ if we used protocol 2 where $\varepsilon_{\text{WB}} = \varepsilon_{\text{BB}}$ throughout the simulation. The similarity between the assembled structures at $\varepsilon_{\text{WB}} = 0.80$ from the two protocols also proves that the results are not kinetically trapped as protocol 2 essentially uses a simulated annealing approach⁶⁷ for both ε_{WB} and ε_{BB} . The disordered clusters are likely arising due to strong polymer-surface binding at $\varepsilon_{\text{WB}} = 0.80$ that dominate the assembly on the surface.

One may wish to compare the morphological changes of the domains on the surface to the changes in shapes of the micelles in the bulk solution. We showed in our recent publication⁵¹ focused on solutions in the absence of a surface, that a higher solvophobic composition of the chain is required for non-spherical micelles to form in the bulk solution. In this study focused on polymers with a symmetric solvophobic-solvophilic composition, we show that all micelles formed in the bulk solution are spherical, regardless of the value of ε_{WB} . As such, the morphological transitions seen on the surface arise only due to the adsorption of the chains on the surface.

To explain the above trends in assembled domains on the surfaces, we dive into the chain packing within the assembled domains on the surfaces. We present both the components of the chain radius of gyration of the solvophobic B-block, parallel ($R_{\text{g,B},\parallel}$) and perpendicular ($R_{\text{g,B},\perp}$) to the surface, for $z = 1$ in **Figure 6**. The increase in $R_{\text{g,B},\parallel}$ with increasing ε_{WB} in **Figure 6a**, indicates that the chains increasingly spread out on the surface. The largest increase in $R_{\text{g,B},\parallel}$ corresponds to the transition from structured domains to disordered interconnected domains (for $\varepsilon_{\text{WB}} = 0.80$), as the surface-B-bead attraction dominates over the B-B interactions that drive the formation of ordered solvophobic B-domains. The decreasing values of $R_{\text{g,B},\perp}$ with increasing ε_{WB} in **Figure 6b** indicates that the solvophobic B-block of the chains flatten nearly completely to the solvophobic surface. The $R_{\text{g,B},\parallel}$ and $R_{\text{g,B},\perp}$ results indicate that the ability of the chains to deform on the surface dictates the resulting assembled structure. We test this hypothesis by increasing the side chain grafting density, z , with the expectation that there would be an exaggeration of the behavior seen at lower values of z due to the shape-persistent nature of the densely grafted bottlebrushes.

To study the impact of side chain crowding on the observed trends in **Figures 4, 5, and 6** we present the results for polymer architectures 2 to 4 with grafting density, $z = 4$. We visualize the resulting assembled structures in **Figure 7** and quantify the structural details for the hemispherical domains in **Figure 8**. As the N_{tot} between the four architectures presented in **Figures 7 and 8** are not the same (refer to Equation 2), we show the effect of increasing the grafting density on each architecture by only comparing the results for $z = 1$ and $z = 4$ for the same architecture.

The two bottlebrush architectures with short side chains ($N_{\text{bb}}=32$ $N_{\text{sc}}=2$ and $N_{\text{bb}}=24$ $N_{\text{sc}}=3$) exhibit the same behavior for $z = 4$ as they do for $z = 1$; at low values of ε_{WB} they form hemispherical domains that increase in size as the value of ε_{WB} increases. At $\varepsilon_{\text{WB}} = 0.30$, the assembled domains only form for $z = 4$. At higher values of ε_{WB} , $\varepsilon_{\text{WB}} = 0.50$ and 0.60 , both architectures transition to continuous ordered stripes; this is in contrast to $z = 1$ where the emergence of stripes either occurs at higher values of ε_{WB} ($N_{\text{bb}}=32$ $N_{\text{sc}}=2$) or there is no evidence of ordered striped domains ($N_{\text{bb}}=24$ $N_{\text{sc}}=3$) at all. For $N_{\text{bb}}=32$ $N_{\text{sc}}=2$, the shift in the transition (from hemispherical to striped domains) to lower values of ε_{WB} is likely due to crowding and a larger number of solvophobic B-beads in the $z = 4$ case compared to the $z = 1$ case. As the number of solvophobic beads in the polymer chain increases, a lower value of ε_{WB} or ε_{BB} is required for adsorption or aggregation as there are more beads within a chain that add up to a larger effective attraction between the surface and other polymer chains.

For the bottlebrush with commensurate side chain and solvophobic backbone length ($N_{\text{bb}}=12$ $N_{\text{sc}}=7$), the higher grafting density ($z = 4$) continues to exhibit the lack of change in the ordered structure with increasing ε_{WB} seen at $z = 1$. The effect of increasing side chain grafting density on aggregation number and domain size is less for this architecture because of the inherently higher crowding of the side chains due to smaller backbone length. This is supported by the observation that at $z = 4$, unlike $z = 1$, the ‘star-like’ polymer architecture ($N_{\text{bb}}=4$ $N_{\text{sc}}=23$) which has the largest crowding near the backbone, behaves similarly to the $N_{\text{bb}}=12$ $N_{\text{sc}}=7$ bottlebrush with similar domain sizes (visually in **Figure 7**), aggregation number (**Figure 8a**), and assembled domain sizes (**Figure 8b**) at lower values of ε_{WB} . These two

architectures only deviate in assembled structure at $\varepsilon_{WB} = 0.60$, where the ‘star-like’ polymer exhibits disordered states (like the $z = 1$ cases at $\varepsilon_{WB} = 0.80$) while the bottlebrush with similar solvophobic backbone and side chain lengths ($N_{bb}=12$ $N_{sc}=7$) does not exhibit disordered states.

Next, we consider the chain conformation at the surface for $z = 4$. $R_{g,B, \parallel}$, in **Figure 9a**, shows the largest increase for the ‘star-like’ polymer architecture ($N_{bb}=4$ $N_{sc}=23$) when the polymer transitions from ordered to disordered domain structures, similar to all of the architectures with $z = 1$; this is because the chains are able to spread out on the solvophobic surface and the surface-B-block attractions dominate over the B-B interactions. The polymer architecture with a similar solvophobic backbone and side chain length ($N_{bb}=12$ $N_{sc}=7$), shows only marginal changes in both $R_{g,B, \parallel}$ and $R_{g,B, \perp}$ (in **Figures 9a-b**, respectively) which indicates that this densely grafted brush cannot adapt its chain conformation on the surface and forms similar domain structures for all values of ε_{WB} investigated. The bottlebrush polymer architectures ($N_{bb}=32$ $N_{sc}=2$ and $N_{bb}=24$ $N_{sc}=3$) show an increase in their $R_{g,B, \parallel}$ when the domain structure transitions from hemispheres to inter-connected disordered domains in **Figure 9a**. The significant decrease in $R_{g,B, \perp}$ with increasing values of ε_{WB} for the bottlebrushes with long side chains and the ‘star-like’ polymers (architectures 2, 3, and 5) in **Figure 9b** indicates that the polymers flatten out on the surface.

Based on the past literature,^{11, 12} we hypothesize that the striped domains at high ε_{WB} are due to an increase in the effective stiffness along the polymer backbone induced by surface adsorption of the chains. The side chains have a smaller volume available to them when adsorbed on the surface than in the bulk solution, effectively increasing the steric repulsion between the side chains and the stiffness along the backbone.^{11, 12} The increase in effective stiffness of the bottlebrush polymers could reduce their ability to adopt favorable conformations for packing into hemispherical domains leading to inter-connected disordered domains that allow for more regular packing of stiffer polymer chains. In **Figure S5**, we plot the persistence length of the solvophobic backbone, $l_{ps,B}$, as a function of increasing values of ε_{WB} under various solvent conditions considering both the chains adsorbed on the surface and chains far away from

the surface in the bulk solution. We calculate $l_{ps,B}$ by modelling the solvophobic block as a wormlike cylinder⁶⁸ which was shown in a recent publication⁶⁹ to accurately describe bottlebrush conformations in dilute solutions. For chains within micelles formed in the bulk solution, $l_{ps,B}$ is independent of the value of ε_{WB} , as expected. For chains adsorbed on the surface that form striped domains, $l_{ps,B}$ increases with increasing ε_{WB} ; see for example the bottlebrush architectures ($N_{bb}=32$ $N_{sc}=2$ and $N_{bb}=24$ $N_{sc}=3$). The increase in $l_{ps,B}$ is more prominent at low values of ε_{BB} (i.e., before assembled domains form on the surface) than at high values of ε_{BB} (i.e., after assembly domains form on the surface) as the packing of the chains influence the chain conformations. In the case of $N_{bb}=24$ $N_{sc}=3$, the $l_{ps,B}$ decreases as ε_{WB} increases when the system transitions from hemispherical to striped domains, similar to the reduction of chain stretching seen in the transition of spherical to cylindrical micelles to alleviate the entropic penalty for chain stretching;⁶⁶ then $l_{ps,B}$ continues to increase with increasing values of ε_{WB} . For architectures that do not show the striped domain formation (i.e., bottlebrush with similar solvophobic backbone and side chain lengths $N_{bb}=12$ $N_{sc}=7$ and ‘star-like’ $N_{bb}=4$ $N_{sc}=23$) the data is not shown as $l_{ps,B}$ exceeds the backbone length making the calculation unreliable.

Even though we have focused our discussion on the solvophobic B block of the polymers, one should note that the solvophilic A block also has a significant role in all the assembled morphologies on the surface. In the assembled state of amphiphilic polymers, the solvophilic A blocks induce steric repulsions in the corona due to excluded volume effects and this excluded volume is a function of the polymer architecture. In the case of the densely grafted bottlebrushes ($z = 4$ for $N_{bb}=24$ $N_{sc}=3$ and $N_{bb}=32$ $N_{sc}=2$), the stiffening of the backbone due to the steric repulsions of the side chains would induce a flat core-corona interface where the polymers are able to pack regularly side-by-side without causing significant steric repulsions between A blocks in the corona. In the case of the ‘star-like’ polymer architecture ($z = 4$ for $N_{bb}=4$ $N_{sc}=23$), the corona A block chains spread out as much as possible, taking up a large volume to relieve the steric repulsions near the grafting point at the core-corona interface. The increased volume of the ‘star-like’ polymer solvophilic A blocks results in a curved core-corona interface as steric repulsion in

the corona prevents a regular side-by-side packing of the chains. Thus, the architecture of solvophilic A block plays an important role in predicting the final assembled state in bulk and on the surface.

To confirm that the trends we emphasize in **Figures 7 – 9** are not specific to those chosen values of N_{tot} , in **Figure S6**, we show results from protocol 2 for polymers with $z = 4$ and an approximately constant N_{tot} . By comparing **Figure S6** with the bottom row of **Figure 7**, where N_{tot} varies between different architectures with $z = 4$, we see that the trend in domain structure with varying polymer architectures with $z = 4$ is the same. The polymer architectures with backbones much longer than their side chain lengths form continuous domains, the polymer architectures with similar solvophobic backbone and side chain lengths form hemispherical domains, and the polymer architectures with backbone lengths much shorter than their side chain lengths form disordered domains on the surface. This confirms that the trends we emphasize in **Figures 7 – 9** are not specific to those chosen values of N_{tot} .

Lastly, in **Figures S7 and S8**, we compare the results from simulations with square-packed surfaces and hexagonal-packed surfaces to demonstrate that the polymer architecture, not the two-dimensional pattern of surface beads on the bottom surface, determines the changing/constant domain shapes as a function of surface-B attraction. The hexagonal-packed surface is overall more attractive than the square-packed surfaces at the same value of ϵ_{WB} as each adsorbing polymer B-bead has more surface bead neighbor contacts at a given coordinate on the surface (**Figure S9**). As a result of the hexagonal-packed surface being more attractive than the square-packed surfaces at the same value of ϵ_{WB} , the structural transitions of the assembled domains on the square-packed surface with increasing ϵ_{WB} occur at lower values of ϵ_{WB} on hexagonal-packed surfaces. At the same value of ϵ_{WB} the adsorbing polymers have larger parallel and smaller perpendicular components of the solvophobic block radius of gyration for the hexagonal-packed surfaces than for the square-packed surfaces (**Figure S8**), but all trends seen on square-packed are also seen on hexagonal-packed surfaces.

4. Conclusions

In this computational paper, we investigate how the self-assembly of varying amphiphilic polymer architectures (linear, bottlebrush, and ‘star-like’) is impacted by surfaces with attraction towards solvophobic polymer chemistry. The branching in polymer architectures affects the polymer conformations and how they pack on the attractive surface resulting in different domain structures near/on solvophobic surfaces. Bottlebrushes with similar solvophobic block backbone and side chain lengths form hemispherical domains on the surface that do not change in size with increasing attraction strength of the surface to the solvophobic block. This is because these densely crowded brushes cannot alter their conformations to make more favorable surface-solvophobic block contacts. On the other hand, bottlebrushes with backbones that are longer than the side chain lengths form hemispherical domains that transition to striped domains and continuous domains as surface-polymer attraction strength increases. This transition in domain structure results from more ordered packing of the chains on the surface due to increased backbone stiffness as the volume available to the side chains of adsorbed polymers is reduced as compared to the bulk solution state far from the surface. Going from bottlebrush to linear or from bottlebrush to ‘star-like’, the domains that form near/on the surface become more sensitive to increasingly attractive surfaces, as the chains are more able to spread out on the surface and pack into larger hemispherical domain structures.

Overall, these results guide the design of assembled structures near/on surfaces by tuning the polymer architecture and the surface chemistry. We show how polymer architecture can be designed to target continuous or discrete domains on solvophobic surfaces with tunable sensitivity to different surface chemistries.

Conflicts of interest

There are no conflicts of interest to declare.

Acknowledgments

We thank the National Science Foundation DMREF program, grant number NSF DMREF-1629156, for their financial support. We thank Karen L. Wooley, Darrin J. Pochan, Bill Johnson, and

students supported by this NSF DMREF grant for their feedback and discussions during the course of this work. The simulations reported in this paper were conducted on the high-performance computing resources of the Farber supercomputing cluster run by the Information Technologies (IT) resources at the University of Delaware and the Stampede cluster as part of the Extreme Science and Engineering Discovery Environment (XSEDE) at the University of Texas under the XSEDE grant TG-MCB100140.

References

1. J. N. Albert and T. H. Epps III, *Materials Today*, 2010, **13**, 24-33.
2. P. M. Claesson, R. Makuska, I. Varga, R. Meszaros, S. Titmuss, P. Linse, J. S. Pedersen and C. Stubenrauch, *Advances in colloid and interface science*, 2010, **155**, 50-57.
3. S. Peleshanko and V. V. Tsukruk, *Progress in Polymer Science*, 2008, **33**, 523-580.
4. R. Verduzco, X. Li, S. L. Pesek and G. E. Stein, *Chem. Soc. Rev.*, 2015, **44**, 2405-2420.
5. G. Xie, M. R. Martinez, M. Olszewski, S. S. Sheiko and K. Matyjaszewski, *Biomacromolecules*, 2018, **20**, 27-54.
6. G. E. Stein, T. S. Laws and R. Verduzco, *Macromolecules*, 2019, **52**, 4787-4802.
7. B. Zhang, F. Gröhn, J. S. Pedersen, K. Fischer and M. Schmidt, *Macromolecules*, 2006, **39**, 8440-8450.
8. S. Rathgeber, T. Pakula, A. Wilk, K. Matyjaszewski and K. L. Beers, *J. Chem. Phys.*, 2005, **122**, 124904.
9. S. Rathgeber, T. Pakula, A. Wilk, K. Matyjaszewski, H. il Lee and K. L. Beers, *Polymer*, 2006, **47**, 7318-7327.
10. S. Elli, G. Raffaini, F. Ganazzoli, E. G. Timoshenko and Y. A. Kuznetsov, *Polymer*, 2008, **49**, 1716-1724.
11. H.-P. Hsu, W. Paul and K. Binder, *The Journal of chemical physics*, 2010, **133**, 134902.
12. H.-P. Hsu, W. Paul and K. Binder, *The Journal of Physical Chemistry B*, 2011, **115**, 14116-14126.
13. P. Linse and P. M. Claesson, *Macromolecules*, 2009, **42**, 6310-6318.
14. A. Naderi, J. Iruthayaraj, A. Vareikis, R. Makuska and P. M. Claesson, *Langmuir*, 2007, **23**, 12222-12232.

15. I. I. Potemkin, *Macromolecules*, 2006, **39**, 7178-7180.
16. H.-P. Hsu, W. Paul and K. Binder, *Macromolecules*, 2013, **47**, 427-437.
17. P. Linse and P. M. Claesson, *Macromolecules*, 2010, **43**, 2076-2083.
18. S. Qin, K. Matyjaszewski, H. Xu and S. S. Sheiko, *Macromolecules*, 2003, **36**, 605-612.
19. M. Alaboalirat, L. Qi, K. J. Arrington, S. Qian, J. K. Keum, H. Mei, K. C. Littrell, B. G. Sumpter, J.-M. Y. Carrillo and R. Verduzco, *Macromolecules*, 2018, **52**, 465-476.
20. H.-Y. Chang, Y.-L. Lin, Y.-J. Sheng and H.-K. Tsao, *Macromolecules*, 2012, **45**, 4778-4789.
21. R. Fenyves, M. Schmutz, I. J. Horner, F. V. Bright and J. Rzayev, *J. Am. Chem. Soc.*, 2014, **136**, 7762-7770.
22. N. G. Fytas and P. E. Theodorakis, *Materials Research Express*, 2014, **1**, 015301.
23. H.-P. Hsu, W. Paul and K. Binder, *EPL (Europhysics Letters)*, 2006, **76**, 526.
24. H.-P. Hsu, W. Paul and K. Binder, *Macromol. Symp.*, 2007, **252**, 58-67.
25. H.-P. Hsu, W. Paul and K. Binder, *Macromol. Theory Simul.*, 2007, **16**, 660-689.
26. H.-i. Lee, K. Matyjaszewski, S. Yu-Su and S. S. Sheiko, *Macromolecules*, 2008, **41**, 6073-6080.
27. Z. Li, J. Ma, C. Cheng, K. Zhang and K. L. Wooley, *Macromolecules*, 2010, **43**, 1182-1184.
28. Z. Li, J. Ma, N. S. Lee and K. L. Wooley, *J. Am. Chem. Soc.*, 2011, **133**, 1228-1231.
29. X. Lian, D. Wu, X. Song and H. Zhao, *Macromolecules*, 2010, **43**, 7434-7445.
30. C. Luo, C. Chen and Z. Li, *Pure and Applied Chemistry*, 2012, **84**, 2569-2578.
31. A. Polotsky, M. Charlaganov, Y. Xu, F. A. M. Leermakers, M. Daoud, A. H. E. Müller, T. Dotera and O. Borisov, *Macromolecules*, 2008, **41**, 4020-4028.
32. Y. Shi, W. Zhu, D. Yao, M. Long, B. Peng, K. Zhang and Y. Chen, *ACS Macro Letters*, 2013, **3**, 70-73.
33. P. E. Theodorakis, W. Paul and K. Binder, *Macromolecules*, 2010, **43**, 5137-5148.
34. P. E. Theodorakis, W. Paul and K. Binder, *The European Physical Journal E*, 2011, **34**, 52.

35. H. Unsal, S. Onbulak, F. Calik, M. Er-Rafik, M. Schmutz, A. Sanyal and J. Rzayev, *Macromolecules*, 2017, **50**, 1342-1352.
36. J. Wang, K. Guo, L. An, M. Müller and Z.-G. Wang, *Macromolecules*, 2010, **43**, 2037-2041.
37. Z. Wang, X. Wang, Y. Ji, X. Qiang, L. He and S. Li, *Polymer*, 2018, **140**, 304-314.
38. P. Xu, H. Tang, S. Li, J. Ren, E. Van Kirk, W. J. Murdoch, M. Radosz and Y. Shen, *Biomacromolecules*, 2004, **5**, 1736-1744.
39. W. F. Daniel, J. Burdyńska, M. Vatankhah-Varnoosfaderani, K. Matyjaszewski, J. Paturej, M. Rubinstein, A. V. Dobrynin and S. S. Sheiko, *Nature materials*, 2016, **15**, 183.
40. S. S. Sheiko, J. Zhou, J. Arnold, D. Neugebauer, K. Matyjaszewski, C. Tsitsilianis, V. V. Tsukruk, J.-M. Y. Carrillo, A. V. Dobrynin and M. Rubinstein, *Nature materials*, 2013, **12**, 735.
41. S. J. Dalsin, T. G. Rions-Maehren, M. D. Beam, F. S. Bates, M. A. Hillmyer and M. W. Matsen, *ACS nano*, 2015, **9**, 12233-12245.
42. Y. Xia, B. D. Olsen, J. A. Kornfield and R. H. Grubbs, *Journal of the American Chemical Society*, 2009, **131**, 18525-18532.
43. C. Hou, J. Hu, G. Liu, J. Wang, F. Liu, H. Hu, G. Zhang, H. Zou, Y. Tu and B. Liao, *Macromolecules*, 2013, **46**, 4053-4063.
44. S. W. Hong, W. Gu, J. Huh, B. R. Sveinbjornsson, G. Jeong, R. H. Grubbs and T. P. Russell, *ACS nano*, 2013, **7**, 9684-9692.
45. B. R. Sveinbjörnsson, R. A. Weitekamp, G. M. Miyake, Y. Xia, H. A. Atwater and R. H. Grubbs, *Proceedings of the National Academy of Sciences*, 2012, **109**, 14332-14336.
46. G. Sun, S. Cho, C. Clark, S. V. Verkhoturov, M. J. Eller, A. Li, A. Pavía-Jiménez, E. A. Schweikert, J. W. Thackeray and P. Trefonas, *Journal of the American Chemical Society*, 2013, **135**, 4203-4206.
47. J. Bolton, T. S. Bailey and J. Rzayev, *Nano letters*, 2011, **11**, 998-1001.
48. L.-C. Cheng, K. R. Gadelrab, K. Kawamoto, K. G. Yager, J. A. Johnson, A. Alexander-Katz and C. A. Ross, *Nano letters*, 2018, **18**, 4360-4369.
49. X. Li, S. L. Prukop, S. L. Biswal and R. Verduzco, *Macromolecules*, 2012, **45**, 7118-7127.
50. S. L. Pesek, Y.-H. Lin, H. Z. Mah, W. Kasper, B. Chen, B. J. Rohde, M. L. Robertson, G. E. Stein and R. Verduzco, *Polymer*, 2016, **98**, 495-504.
51. M. G. Wessels and A. Jayaraman, *Soft matter*, 2019, **15**, 3987-3998.

52. D. Ceperley, M. H. Kalos and J. L. Lebowitz, *Phys. Rev. Lett.*, 1978, **41**, 313-316.
53. G. S. Grest and K. Kremer, *Phys. Rev. A*, 1986, **33**, 3628-3631.
54. I. Lyubimov, M. G. Wessels and A. Jayaraman, *Macromolecules*, 2018, **51**, 7586-7599.
55. J. E. Jones, *Proc R Soc Lond A Math Phys Sci*, 1924, **106**, 441-462.
56. J. D. Weeks, D. Chandler and H. C. Andersen, *J. Chem. Phys.*, 1971, **54**, 5237-5247.
57. S. Metzger, M. Müller, K. Binder and J. Baschnagel, *Macromolecular theory and simulations*, 2002, **11**, 985-995.
58. D. J. Beltran-Villegas and A. Jayaraman, *Journal of Chemical & Engineering Data*, 2018, **63**, 2351-2367.
59. D. J. Beltran-Villegas, I. Lyubimov and A. Jayaraman, *Molecular Systems Design & Engineering*, 2018, **3**, 453-472.
60. M. Dong, M. G. Wessels, J. Y. Lee, L. Su, H. Wang, R. A. Letteri, Y. Song, Y.-N. Lin, Y. Chen and R. Li, *ACS nano*, 2019, **13**, 5147-5162.
61. I. Lyubimov, D. J. Beltran-Villegas and A. Jayaraman, *Macromolecules*, 2017, **50**, 7419-7431.
62. S. Plimpton, *Journal of computational physics*, 1995, **117**, 1-19.
63. W. G. Hoover, *Physical review A*, 1985, **31**, 1695.
64. M. E. J. Newman and R. M. Ziff, *Phys. Rev. E*, 2001, **64**, 016706.
65. W. Humphrey, A. Dalke and K. Schulten, *Journal of molecular graphics*, 1996, **14**, 33-38.
66. E. B. Zhulina, M. Adam, I. LaRue, S. S. Sheiko and M. Rubinstein, *Macromolecules*, 2005, **38**, 5330-5351.
67. S. Kirkpatrick, C. D. Gelatt and M. P. Vecchi, *science*, 1983, **220**, 671-680.
68. H. Benoit and P. Doty, *The Journal of Physical Chemistry*, 1953, **57**, 958-963.
69. S. Dutta, T. Pan and C. E. Sing, *Macromolecules*, 2019, **52**, 4858-4874.

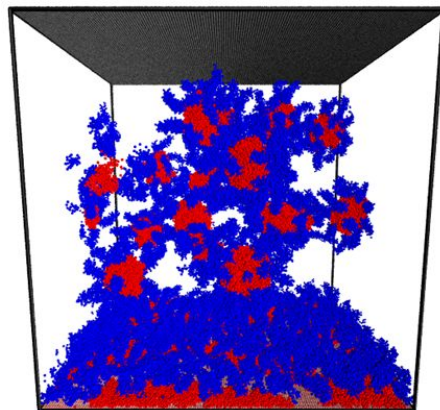


Figure 1. Image of the simulation box. The solvophobic B beads of amphiphilic polymers are represented in red and the solvophilic A beads in blue. The top neutral surface is represented with gray beads and the bottom attractive surface is represented with light red beads. The distance between the top and bottom surface is large enough to allow for bulk-like polymer assembly in between the surfaces.

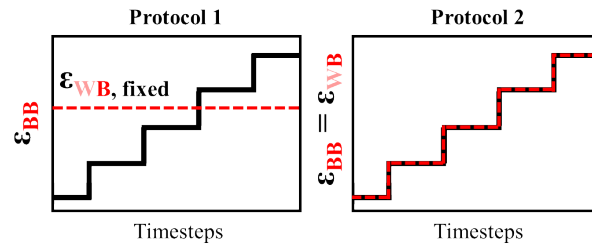


Figure 2. Simulation schemes to represent solvophobic surfaces that differ from the solvophobic bead and do not change significantly with changing solvent quality (protocol 1) and solvophobic surface that has the same bead type as the solvophobic bead (protocol 2).

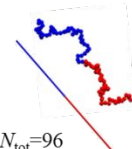
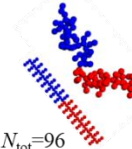
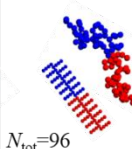
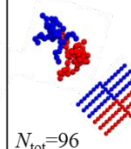
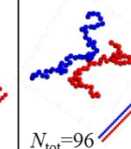
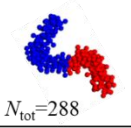
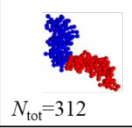
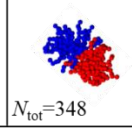
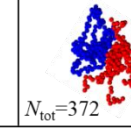
		Polymer architecture				
Grafting density		$N_{bb}=96$ $N_{sc}=0$	$N_{bb}=32$ $N_{sc}=2$	$N_{bb}=24$ $N_{sc}=3$	$N_{bb}=12$ $N_{sc}=7$	$N_{bb}=4$ $N_{sc}=23$
$z = 1$		 $N_{tot}=96$	 $N_{tot}=96$	 $N_{tot}=96$	 $N_{tot}=96$	 $N_{tot}=96$
$z = 4$			 $N_{tot}=288$	 $N_{tot}=312$	 $N_{tot}=348$	 $N_{tot}=372$

Figure 3. Schematics of the polymer architectures in this study with grafting densities $z = 1$ and $z = 4$. The solvophobic B-beads are represented in red and the solvophilic A-beads are represented in blue. In the top row, for $z = 1$, we maintain a constant number of beads per chain ($N_{tot}=96$) for all architectures as we go from left to right; to accomplish this we decrease the backbone length (N_{bb}) and simultaneously increasing the side chain length (N_{sc}). In the bottom row, for $z = 4$, the backbone and side chain lengths are the same as the branched polymers in the top row; the number of side chains per backbone bead is 4 compared to 1 in the top row.

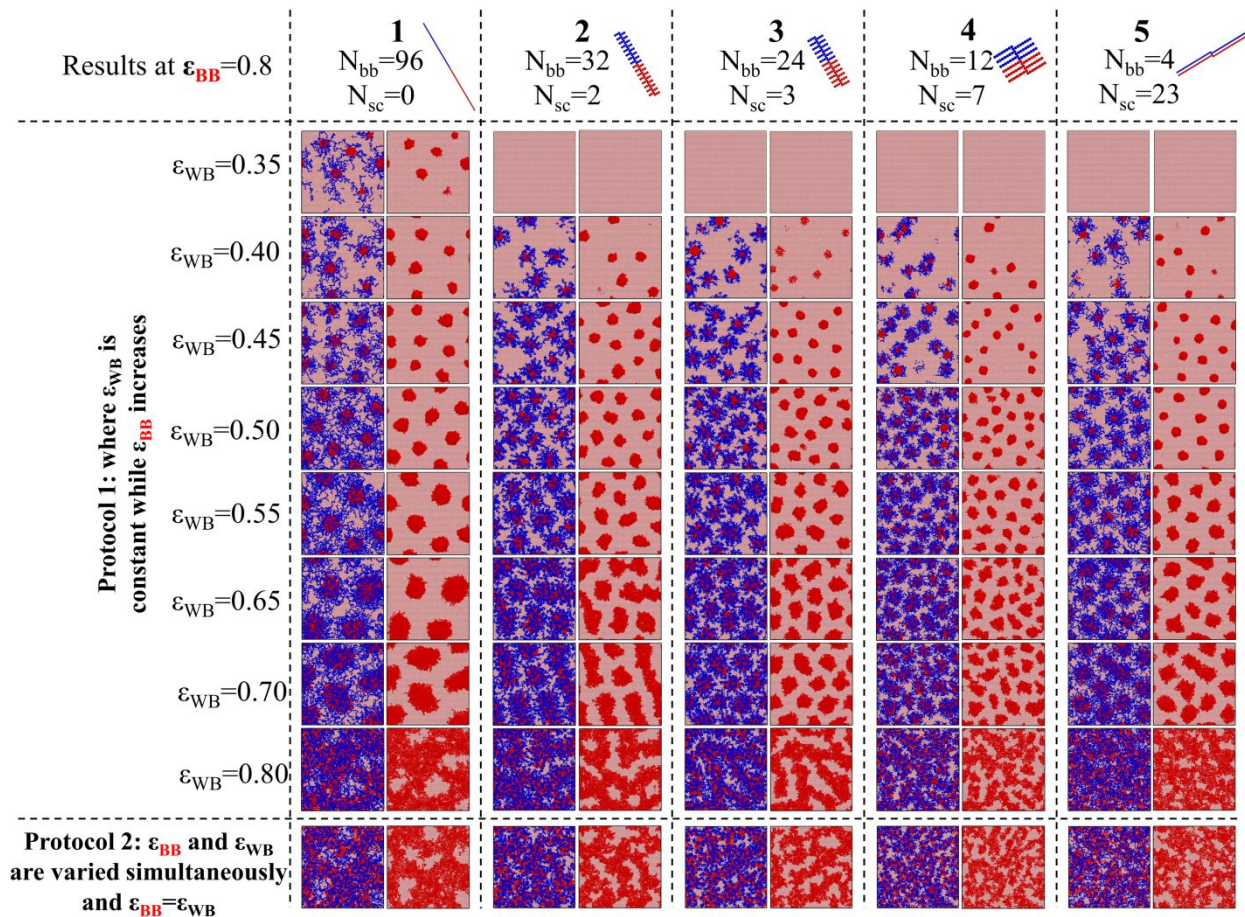


Figure 4. Assembled domains for polymer architectures 1 through 5 with $z = 1$ and $N_{tot} = 96$ on solvophobic surfaces with different fixed values of ϵ_{WB} (rows) as ϵ_{BB} is varied (protocol 1). The bottom row shows analogous results as the top rows but with protocol 2 where ϵ_{WB} and ϵ_{BB} are kept equal and varied simultaneously. All images shown are for $\epsilon_{BB} = 0.8$. For each architecture, all beads are shown on the left and the solvophilic beads are hidden on the right to show the solvophobic domains clearly.

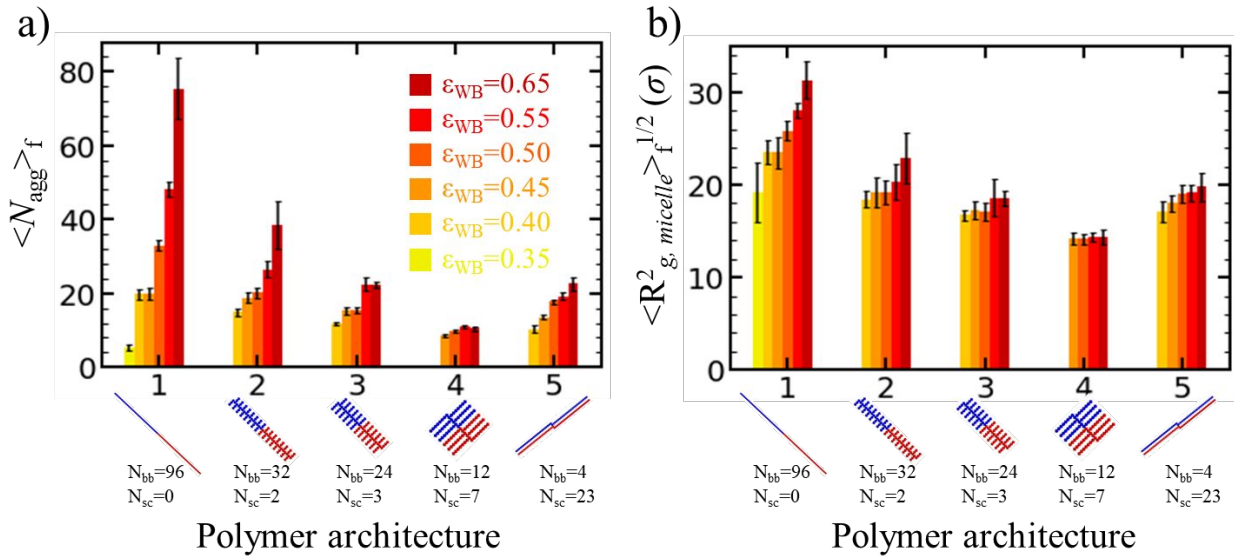


Figure 5. Structural characteristics of hemispherical adsorbed domains for polymer architectures with $z = 1$ at different fixed values of ϵ_{WB} . (a) The aggregation number and (b) micelle radius of gyration of the domains near/at the surface at $\epsilon_{BB} = 0.8$.

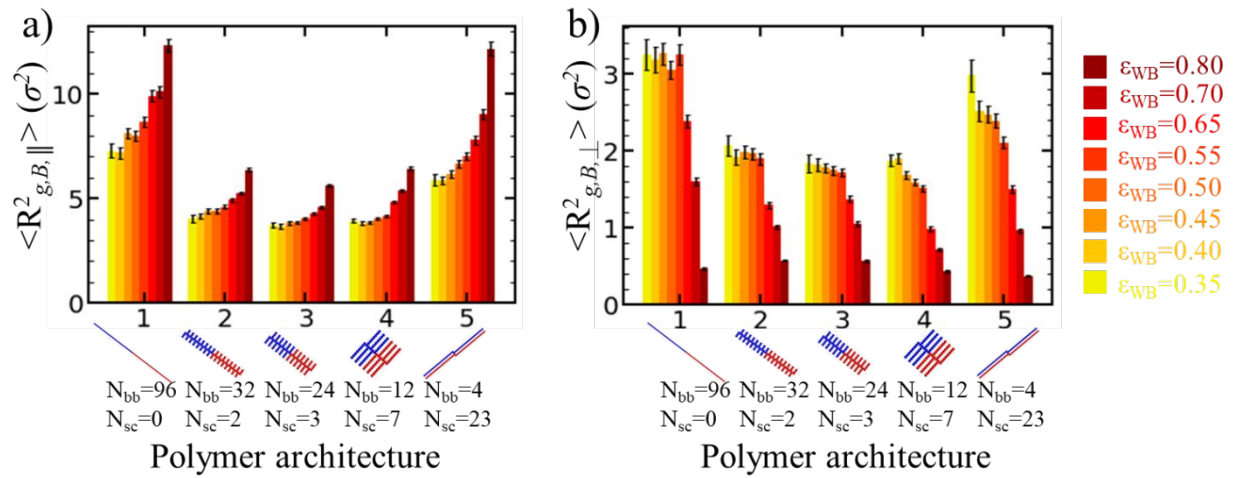


Figure 6. Adsorbed chain structural characteristics for polymer architectures with $z = 1$ at different fixed values of ϵ_{WB} with the parallel (a) and perpendicular (b) components of the radius of gyration of the solvophobic block at $\epsilon_{BB}=0.8$.

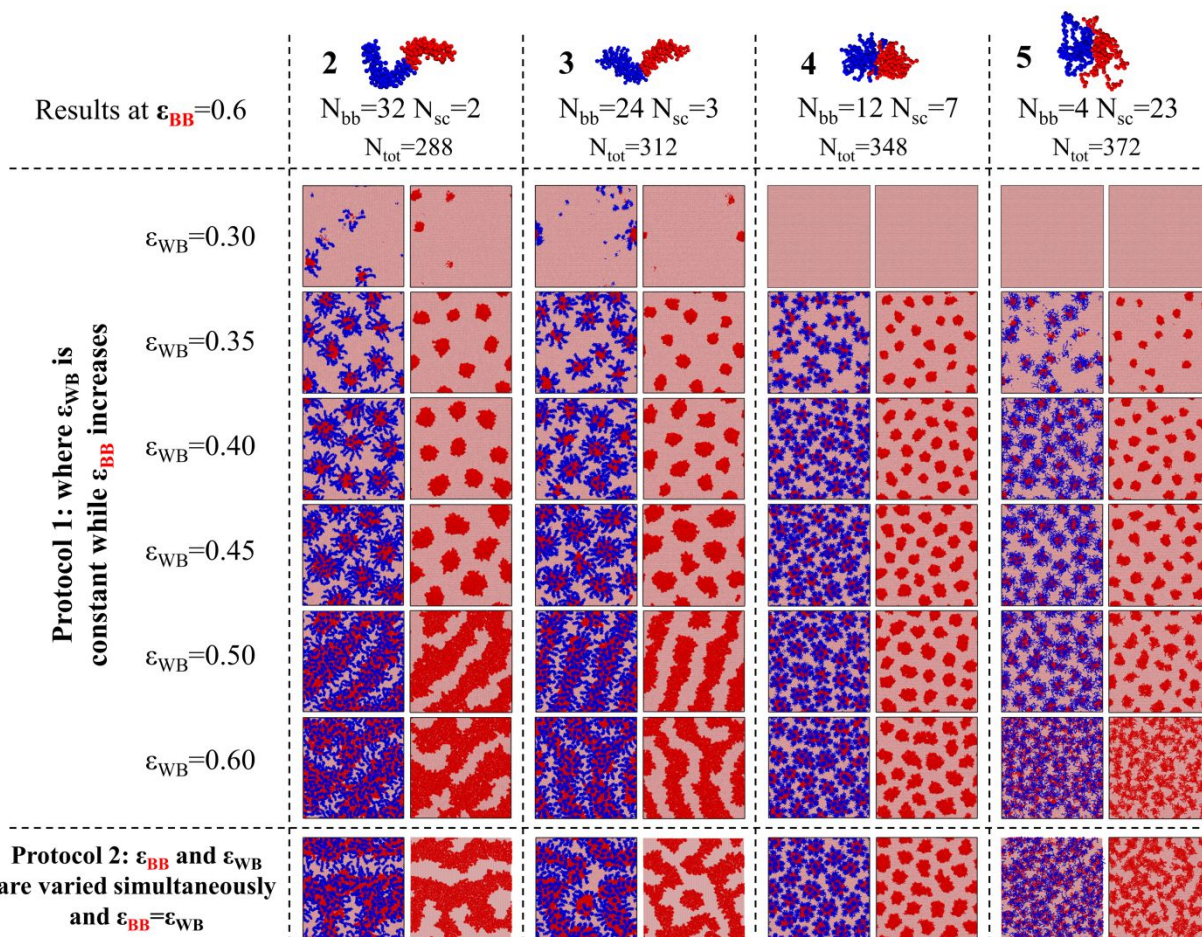


Figure 7. Assembled domains for polymer architectures 2 through 5 with $z = 4$ and varying N_{tot} (for architectures 2 through 5 $N_{tot} = 288, 312, 348,$ and 372 , respectively) on solvophobic surfaces with different fixed values of ϵ_{WB} (rows) as ϵ_{BB} is varied (protocol 1). The bottom row shows analogous results as the top rows but with protocol 2 where ϵ_{WB} and ϵ_{BB} are kept equal and varied simultaneously. All images shown are for $\epsilon_{BB} = 0.6$. For each architecture, all the beads are shown on the left and the solvophilic beads are hidden on the right to show the solvophobic domains clearly.

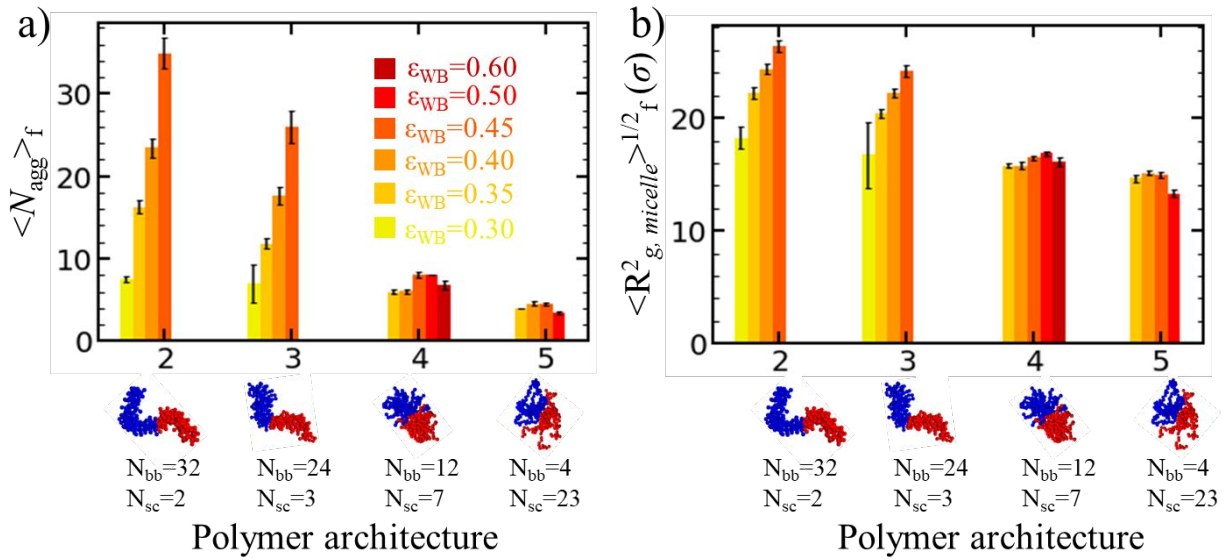


Figure 8. Structural characteristics of adsorbed clusters for polymer architectures with $z = 4$ at different fixed values of ϵ_{WB} . (a) The aggregation number of adsorbed clusters at $\epsilon_{BB} = 0.8$. (b) The micelle radius of gyration of adsorbed clusters at $\epsilon_{BB} = 0.6$.

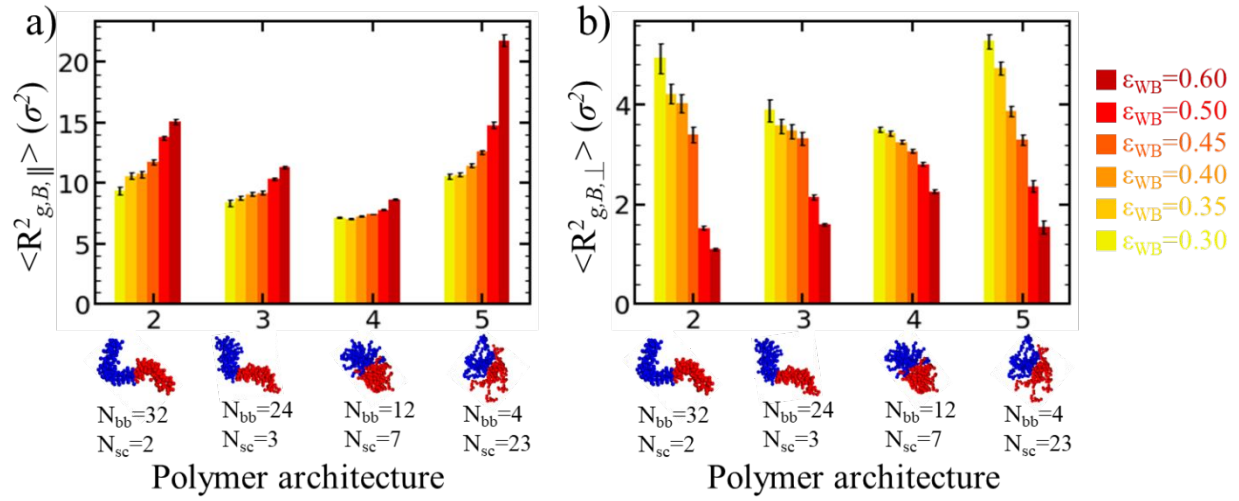


Figure 9. Adsorbed chain structural characteristics for polymer architectures with $z = 4$ at different fixed values of ϵ_{WB} with the parallel (a) and perpendicular (b) components of the radius of gyration of the solvophobic block at $\epsilon_{BB} = 0.6$.

for **Table of Contents** use only

